Free Energy Landscape and Rate Estimation of the Aromatic Ring Flips in Basic Pancreatic Trypsin Inhibitor Using Metadynamics

Mandar Kulkarni and Pär Söderhjelm**

Division of Biophysical Chemistry, Lund University, Chemical Center, 22100 Lund, Sweden

KEYWORDS: Aromatic ring flip, Metadynamics, Kinetics, Infrequent metadynamics, BPTI

ABSTRACT: Aromatic side-chains (phenylalanine and tyrosine) of a protein flip by 180° around the $C_\beta - C_\gamma$ axis (χ_2 dihedral of side-chain) producing two symmetry-equivalent states. The ring-flip dynamics act as an NMR probe to understand local conformational fluctuations. Ring-flips are categorized as slow (ms onwards) or fast (ns to near ms) based on timescales accessible to NMR experiments. In this study, we investigated the ability of the infrequent metadynamics approach to discriminate between slow and fast ring-flips for eight individual aromatic side-chains (F4, Y10, Y21, F22, Y23, F33, Y35, F45) of basic pancreatic trypsin inhibitor (BPTI). Well-tempered metadynamics simulations were performed to observe ring-flipping free energy surfaces for all eight aromatic residues. The results indicate that χ_2 as a standalone collective variable (CV) is not sufficient to classify fast and slow ring-flips. Most of the residues needed χ_1 $(N - C_\alpha)$ as a complementary CV, indicating the importance of

librational motions in ring-flips. Multiple pathways and mechanisms were observed for residues F4, Y10, and F22. Recrossing events are observed for residues F22 and F33, indicating a possible role of friction effects in the ring-flipping. The results demonstrate the successful application of the metadynamics based approach to estimate ring-flip rates of aromatic residues in BPTI and identify certain limitations of the approach.

INTRODUCTION

The fluctuations of protein residues in its native state produce an ensemble of interconvertible substates.[1] These dynamic protein fluctuations occur over a wide range of timescales. For example, the ring-flip motions (180º rotation around C_β-C_γ axis) of aromatic side-chains in globular proteins occur from nanoseconds[2] to seconds[3]. The presence of different timescales for aromatic ring-flipping in proteins was initially observed in seminal NMR studies by Wüthrich and co-workers[4-5] while studying the internal dynamics of basic pancreatic trypsin inhibitor (BPTI). The value of the side-chain torsion angle χ_2 (C_α-C_β-C_γ-$C_{\delta1}$ / CA-CB-CG-$CD1$ in figure 1) acts as an indicator of aromatic ring-flipping. The ring-flipping process occasionally involves librational motions relative to backbone atoms, identified using the χ_1 (N-C_α-C_β-C_γ / N-CA-CB-CG) torsion. The aromatic side-chains are often utilized as internal NMR probes to understand the protein interior dynamics surrounding these side-chains[6-9].

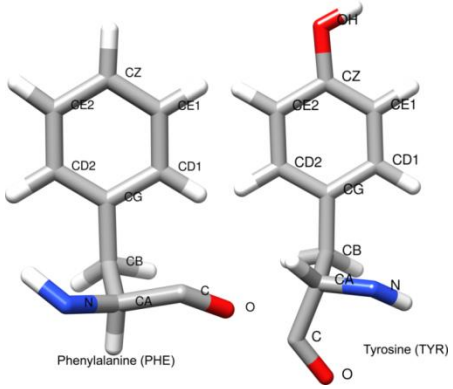

Figure 1. Atom names of tyrosine and phenylalanine indicating torsion χ_2 (CA-CB-CG-$CD1$) and χ_1 (N-CA-CB-CG).

The ring-flips are not directly associated with any biological functions[10] but rely on transient packing defects around the aromatic ring, which might be relevant to small-molecule binding or internal protein hydration. The ring flipping event in the protein interior is associated with breathing motion, a transient cavity expansion exposing the protein interior. Such breathing motions provide a transient formation of the necessary volume (*activation volume*[9, 11]) required for the aromatic ring flip. This is a well-established model often referred to as the "cavity model"[12]. The earlier ring-flipping studies proposed a "diffusion model"[13-14] based on Kramer's theory assuming ring-flipping is a diffusion-limited process originating from the frictional effects exerted by surrounding atoms.

In this study, we investigated four tyrosine (Y10, Y21, Y23, and Y35) and four phenylalanine (F4, F22, F33, and F45) residues of BPTI. These aromatic side-chains contribute significantly to the stability of BPTI and mutations[15-17] at these sites with alanine or leucine destabilized protein at room temperature. The NMR investigation of the globular protein BPTI by Wagner et al.[5] was the first study to distinguish slow and fast flipping rings. In general, the aromatic ring flips are classified[5, 18] as slow flips ($k_{flip} \leq 10^3\ s^{-1}$ i.e. $t_{flip} \geq 10^{-3}$ s) and fast flips ($k_{flip} > 10^3\ s^{-1}$ i.e. $t_{flip} < 10^{-3}$ s) based on the flipping time (t_{flip}) accessible to NMR methods. Experimentally, only slow ring flips can be studied using ^{13}C CPMG relaxation experiments[3, 11] by observing signal splitting of symmetrically located δ or ε nuclei on the ring[4] (CD1, CD2, CE1, CE2 positions in figure 1). Experimental NMR studies of BPTI using ^{13}C relaxation dispersion[3] observed that the slow flipping rings Y23, Y35, and F45 in BPTI exhibit an activation enthalpy around 20 kcal/mol. The abundance of experimental observations related to

all eight aromatic residues in BPTI makes it a suitable model system to understand the thermodynamics and kinetics of the ring-flipping mechanism.

Presently, it is possible to perform molecular dynamics (MD) simulations up to a few microseconds within a reasonable time due to advances in computing power and GPU based molecular dynamics codes. In a 1-ms-long BPTI (Amber99SB-I protein force field and TIP4P-Ew water model) simulation by D.E. Shaw Research (DESRES), ring-flipping was observed for seven out of eight aromatic side-chains.[19] The sparsity of ring-flip events in DESRES simulation suggests that the ring-flipping of aromatic side-chains in BPTI is a rare event. The sampling problem of rare events is generally resolved using enhanced sampling techniques such as metadynamics[20-21]. In this study, well-tempered metadynamics[20] (WTMetaD) simulations are performed to understand the free energy landscape of ring-flipping for all eight aromatic side-chains of BPTI. The successful application of metadynamics provides thermodynamic and structural details of the stable states. However, it is not trivial to evaluate the overall kinetics of the process using such a nonequilibrium approach. Acceleration of rare event by the application of an external biasing potential corrupts the actual dynamics of the process. Recently, the infrequent metadynamics[22] method (InMetaD) was proposed to recover accurate transition times from slowly or *infrequently* biased metadynamics simulations. We performed InMetaD[22] simulations to obtain the first-passage times for transitions between symmetry-equivalent flipped configurations. Analysis of the simulations allows us to propose the ring-flipping mechanism, identify intermediates, and calculated ring-flip rates.

METHODOLOGY

Simulation setup

The initial coordinates for the basic pancreatic trypsin inhibitor (BPTI) were obtained from PDB ID 5PTI, and deuterium atoms and water molecules were removed. The ionizable residues were modeled based on their state at pH 7. The system was built using the tleap module of $AmberTools18$ and then converted to $GROMACS$ format using $ACPYPE$ python script[23]. The protein molecule was modeled using the AMBER ff14SB[24] force field. The protein was first placed in the octahedron box and was solvated by 4302 four-point TIP4P-Ew[25] water molecules. Then, six Cl^- ions were added to neutralize the system. The Joung-Cheatham parameters[26] for chloride ions were used. The distance between walls and protein was 10 Å. All simulations were performed with a time step of 2 fs, and all covalent bonds were constrained using the LINCS algorithm. A cut-off distance of 10 Å was used for short-range Coulomb and Lennard-Jones interactions. A long-range dispersion correction to the energy and pressure was applied. The long-range electrostatic interactions were treated with PME and Fourier grid spacing of 1.2 Å with fourth-order spline interpolation. Periodic boundary conditions were applied, and the system was equilibrated first using the isothermal-isobaric (NPT) ensemble for 1.2 ns. During equilibration, the Berendsen[27] thermostat and barostat were used to maintain 300 K temperature and 1 bar pressure. A restraining force of 25 kcal mol^{-1} $Å^{-2}$ was used on heavy protein atoms during this stage. Then the structure was minimized using the steepest-descent method. The restraining force was reduced to 5 kcal mol^{-1} $Å^{-2}$ and NPT equilibration was performed for 1 ns, followed by system minimization. After this stage, a 10 ns NPT equilibration run was performed using the Parrinello-Rahman barostat[28] (coupling constant 1.0 ps) and Bussi-Donadio-Parrinello's V-rescale[29] thermostat (coupling constant 0.5 ps). The compressibility was set to 4.5

x 10^{-5} bar^{-1}. The structure was minimized, and 100 ns of unbiased simulation was performed (NVT ensemble). A preliminary analysis was performed on this simulation to understand local fluctuations in BPTI. No aromatic ring-flipping was observed during this simulation. The last structure of this simulation was utilized further for metadynamics simulation as well as for all InMetaD simulations. All metadynamics simulations were performed in the NVT ensemble (T=300 K) using $GROMACS$ 2018.3[30-31] and $PLUMED$ 2.5[32-34].

We have also tested the effect of the force field on ring-flipping for residue F22 using (i) CHARMM36m and charmm TIP3P water model (referred to as c36m) and (ii) CHARMM36 and standard TIP3P water model (referred to as c36). In c36m and c36 simulations, all covalent bonds involving hydrogen were constrained using LINCS. The long-range dispersion correction to energy and pressure was absent for CHARMM c36 and c36m simulations. For CHARMM simulations, the PME method was used to calculate long-range electrostatic interactions with a 12 Å cut-off. The Lennard-Jones interactions were smoothly switched to zero between 10 Å and 12 Å.

Metadynamics Simulations

The experimentally fast flipping residues exhibit microsecond to near milliseconds timescales[3], which are still difficult to access by standard molecular dynamics simulations. We have performed WTMetaD simulations to understand the aromatic ring-flipping mechanism and to observe possible intermediate states along the flipping pathway. The details of the metadynamics simulations are reported in Table 1. A cartesian coordinates (R^N) based high dimensional free energy landscape of the system of interest is often studied using low dimensional or coarse-grained descriptors of the coordinate space, $s(R^N)$, called collective variables (CVs). The selection of CVs is critical to correctly capture the underlying free energy landscape and all

possible metastable states. In the present study, the χ_2 dihedral angle was the obvious choice to enhance ring-flipping. In addition, most WTMetaD simulations needed the χ_1 torsion to observe convergence as librational motions relative to the backbone are needed for ring flipping.

Table 1. List of CVs and details of metadynamics parameters; hill width (σ), hill height (w, kJ.mol^{-1}), bias factor (γ), frequency of hill addition (ν , ps). For WTMetaD, ν is 1 ps.

			WTMetaD		InMetaD		
residue	CV	σ	γ	w	γ	w	ν[a]
F4	χ_2 , χ_1	0.07, 0.07	12	1.2	12	0.6	12
Y10	χ_2 , χ_1	0.07,0.07	12	1.2	12	0.3	10
Y21	χ_2	0.07	10	0.6	10	0.6	18
F22	χ_2 , χ_1	0.07,0.07	12	1.2	8	1.2	12
F22 (c36)[a]	χ_2 , χ_1	0.07,0.07	12	1.2	8	0.3	12
F22 (c36m)[b]	χ_2 , χ_1	0.07,0.055	12	1.2	n.a.*	n.a.	n.a.
Y23	χ_2, CMAP	0.07,0.30	12	1.2	10	0.6	8
F33	χ_2 , χ_1	0.07,0.07	8	1.2	10	0.6	12
Y35[c]	χ_2 , χ_1	0.07,0.07	12	1.2	12	0.6	12
F45	χ_2 , χ_1	0.07,0.07	12	1.2	10	0.6	8
F45 (c36)	χ_2 , χ_1	0.07,0.07	n.a.	n.a.	12	0.6	8

[a]charmm36/standard TIP3P simulations, [b]charmm36m/charmm TIP3P, [c]non-converged free energy surface. *n.a.: simulations not performed in this case.

For residue Y23, a contact-map based collective variable was used along with χ_2. This variable is defined using the following function

$$CMAP = \sum_{i=1}^{5} s_i(r) \qquad [1]$$

where $s_i(r)$ is a switching function for each atom pair considered.

$$s(r) = \frac{1-\left(\frac{r-d_0}{r_0}\right)^n}{1-\left(\frac{r-d_0}{r_0}\right)^m}, \qquad n=4, m=8 \qquad [2]$$

The values of r_0 and d_0 are mentioned in **Table S1 in SI** and are based on equilibrium distances (obtained from unbiased simulation) between C_α atoms of five residue pairs viz. A25-G28, G28-G56, C55-A25, C55-C5, A25-C5. We note that such a contact map based collective variable is heuristic, and it is probably possible to define a better CV. For all WTMetaD simulations, the hill width was chosen as one half of the standard deviation of the CV in a free simulation run. The hills were added at an interval of 1 ps.

In some simulations, repulsive harmonic wall bias was (V_b) imposed to restrict sampling up to specific values of either χ_2 or χ_1 values.

$$V_b = k(s-s_0)^2 \qquad [3]$$

where k is the force constant in kJ mol^{-1} rad^{-2}, s_0 limiting the value of χ_2 or χ_1 in radians. $UPPER\_WALLS$ and $LOWER\_WALLS$ keywords in PLUMED are used to avoid sampling above and below the specific limiting value s_0, respectively. The details of parameters k and s_0 are provided in Table S3 in SI.

A time-dependent metadynamics bias $V(s,t)$ corrected with time-dependent bias offset[35] $c(t)$ was used for reweighting[36]. The expression of $c(t)$ is shown below:

$$c(t) = \frac{1}{\beta}\log\frac{\int ds\, e^{-\beta F(s)}}{\int ds\, e^{-\beta\left(F(s)+V(s,t)\right)}} \qquad [4]$$

The evolution of $c(t)$ with simulation time is shown in **figure S1 of SI** to understand the quasi-equilibrated region in WTMetaD simulations. We also tested the variational approach to conformational dynamics[37] (VAC-MetaD) approach to avoid misleading results due to

suboptimal CVs (see Appendix II in SI for further details). The quasi-equilibrated part was utilized in the case of residue F22 and F33 to build CVs using VAC-MetaD[37].

NMR experiments[38-39] have observed that the C14 χ_1 motions are 30-fold faster than C38 χ_1 and lead to low populated state m and a highly populated state M. The disulfide bond orientations arising due to rotations of χ_1 torsion of C14 and C38 residues in BPTI is known as disulfide bond isomerization. The DESRES simulation observed five long-lived BPTI conformational states, with each state having different C14-C38 disulfide bond conformation. The ring-flipping rates were different in each state, suggesting a relation between C14-C38 disulfide bond isomerization and ring-flipping in BPTI. We reweighted the histogram of χ_1(C14) - χ_1(C38) and χ_2(C14)- χ_2(C38) to understand BPTI conformations sampled in converged WTMetaD simulations.

Estimation of the flipping rate from metadynamics simulation

The reliability of InMetaD depends on two major factors viz. (i) chosen collective variables should discriminate between metastable states, (ii) no bias should be deposited in the transition state (TS) region. The converged free energy surface along biased CVs indicates the sampling along possible slow degrees of freedom, which are the bottleneck for the sampling. The same set of collective variables can be utilized for the InMetaD simulations. The criterion to avoid bias addition at the TS region can be achieved by a slow (infrequent) addition of gaussian bias during metadynamics. In all cases, we have performed InMetaD simulations by biasing the χ_2 torsion first. These simulations allowed us to understand the efficiency of χ_2 alone to capture ring-flipping dynamics. InMetaD approach to obtain kinetic information simulations is still in infancy. Previous studies[41-43] have demonstrated the efficiency of this approach to study millisecond timescale dynamics in protein-ligand interactions. For each residue, N independent

simulations were performed to obtain transition times, where $N = 40$ if not otherwise stated. For each i[th] individual run, the acceleration factor[22] (α_i) arising due to slow addition of time-dependent bias along CV s is given as:

$$\alpha_i = \langle e^{\beta V_i(s,t)} \rangle \quad [5]$$

The exponentiated bias is averaged until the time of transition to another basin, i.e., actual simulation time (t_i^{MD}), and the transition times (τ_i) of 180° ring flip is obtained as

$$\tau_i = \alpha_i * t_i^{MD} \quad [6]$$

The average transition time (μ) from multiple transition times (τ_i) is obtained as:

$$\mu = \frac{1}{N}\sum_{i=1}^{N} \tau_i \quad [7]$$

The transition times obtained from InMetaD should follow a Poisson distribution according to the law of rare events. Salvalaglio *et al.*[40] proposed a two-sample Kolmogorov-Smirnov test (KS test) to compare the distribution of transition times (τ_i) to the ideal Poisson distribution. In KS-test, the characteristic ring-flip time (t_{flip}) is obtained by fitting the theoretical cumulative distribution function (TCDF) to the empirical cumulative distribution function of InMetaD derived τ_i values.

$$TCDF = 1 - exp\left(-\frac{t}{t_{flip}}\right) \quad [8]$$

This goodness of fit test helps to understand the deviation of simulated transition times from Poisson characteristics by observing the ratio of average transition time (μ) to the median of transition times τ_i (t_m), and the p-value (significance level 0.05). If the τ_i values follow a Poisson distribution; the ratio $\mu \ln 2/t_m$ should be equal to 1. This ratio is sensitive to the deviation from the Poisson distribution and is reported in the present study along with p-values. The

inverse of fitted t_{flip} value is considered as the flipping rate (k_{flip}) as it has been observed to converge faster[40] than the average (μ) in a previous study[40].

$$k_{flip} = \frac{1}{t_{flip}} \qquad [9]$$

The InMetaD simulations were stopped when the trajectory crosses the barrier and transit to the stable state of interest (i.e., either 180° flipped state or intermediate) by implementing boundary conditions based on biased CV values. The boundary conditions are defined closer to the product using the COMMITOR keyword in PLUMED and not precisely at the speculated transition state CV values. The boundary CV values are monitored at every 10 ps or 50 ps. This protocol assures a complete transition to a flipped state and is not misinterpreted due to recrossing events. In the recrossing events, the trajectory does not continue to the flipped state after crossing a barrier but rather transit back to the starting state minima.

RESULTS AND DISCUSSION

We characterized aromatic ring flipping in BPTI in two complementary ways. First, we used the well-tempered metadynamics (WTMetaD) simulations to calculate the free-energy surface and determine the most relevant intermediates. Second, we used the InMetaD method to calculate flipping rates and distinguish various mechanisms. An important part of the investigation consisted of choosing suitable collective variables (CVs) to be biased in both types of simulations.

The overall results obtained from the InMetaD investigation of each residue are shown in Table 2, together with the corresponding CVs used. The experimental ring flip rates[3] (k_{exp}) at 300 K and rates obtained from 1-ms-long DESRES simulation (k_{des}) are also shown for comparison. We used the procedure in ref. 3 to calculate k_{exp} values.

Table 2. InMetaD derived ring flip time from exponential fit (t_{flip}) at 300 K, ring flip rate ($\boldsymbol{k}_{flip}$), KS-test p-value and the ratio of average (μ) to a median of Poisson distribution from InMetaD simulations, experimental ring flip rate (k_{exp}) at 300 K, and from a 1-ms-long DESRES trajectory (k_{des}).

Residue	CVs	t_{flip} (s)	$k_{flip}(s^{-1})$	p-value	μ ln 2/t_m	$k_{exp}\,(s^{-1})$	$k_{des}\,(s^{-1})$
F4	χ_2 , χ_1	2.80×10^{-5}	3.57×10^{4}	0.32	1.79	$> 10^3$	7.0×10^{6}
Y10	χ_2 , χ_1	5.80×10^{-5}	1.72×10^{4}	0.80	1.54	$> 10^3$	1.0×10^{6}
Y21	χ_2	5.20×10^{-3}	1.92×10^{2}	0.68	1.32	< 100[a]	1.0×10^{3}
F22	χ_2 , χ_1	2.41×10^{-2}	4.15×10^{1}	0.16	3.54	670[b]	7.0×10^{4}
F22 (c36)[d]	χ_2 , χ_1	5.45×10^{-4}	1.83×10^{3}	0.69	1.24	670[b]	7.0×10^{4}
Y23	χ_2, CMAP	9.81×10^{-1}	1.02	0.09	1.80	140[c]	1.0×10^{3}
F33	χ_2 , χ_1	3.50×10^{-5}	2.86×10^{4}	0.03	2.47	$> 10^3$	6.0×10^{6}
Y35	χ_2 , χ_1	3.49	2.87×10^{-1}	0.58	3.22	4[c]	1.0×10^{4}
F45	χ_2 , χ_1	3.22	3.11×10^{-1}	0.95	1.44	220[c]	0
F45 (c36)[e]	χ_2 , χ_1	1.78×10^{-1}	5.61	0.97	1.40	220[c]	0

[a]308 K, [b]278 K, [c]values estimated using the Arrhenius equation and with data from Ref. [3], results from [d]16 simulations and [e]12 simulations.

Free Energy and Flipping Mechanism

The results for all eight residues are mentioned in this section. For all free energy profiles, the position of the starting configuration is denoted with state A and intermediates with I_n (n=1,2). The corresponding symmetry-equivalent states are indicated with prime notation (A' and I_n', n=1,2). Representative structures of A and I_n states are shown for each residue. The convergence of metadynamics simulations and diffusion along CVs for each simulation are shown in supporting information (**figures S2 to S10**). The distributions of InMetaD trajectory endpoints

immediately after flipping (started from state A) in each case are shown in figures **S11 and S12 in SI**. Following the NMR-motivated "fast" and "slow" classification of aromatic ring flips, the fast-flipping residues (F4, F33, and Y10) are described first, and the remaining slow flipping residues are described later. However, note that the fast-flipping rings in the BPTI exhibit t_{flip} values on the microsecond time scale, making it challenging to obtain statistically significant results. Residues F4 and Y10 (among other residues) could flip via multiple pathways; the t_{flip} values and KS-test derived parameters for each mechanism are mentioned in **Table 3.**

Fast flipping residues

Table 3. Mechanism Dependent Results of the Infrequent Metadynamics Simulations of Residue F4 and Y10.

Residue	mechanism	N_{traj}[a]	$t_{flip}\,(s)$	$k_{flip}(s^{-1})$	p-value	μ ln 2/tm
F4	All	40	2.80×10^{-5}	3.57×10^{4}	0.32	1.79
	$A \rightleftharpoons I1 \rightleftharpoons I1' \rightarrow A'$	22	3.02×10^{-5}	3.31×10^{4}	0.82	1.48
	$A \rightleftharpoons I1 \rightarrow I2'$	6	2.21×10^{-5}	4.52×10^{4}	0.71	0.80
	$A \rightarrow A'$	12	2.81×10^{-5}	3.56×10^{4}	0.13	2.78
Y10	All	40	5.80×10^{-5}	1.72×10^{4}	0.80	1.54
	$A \rightleftharpoons I1 \rightarrow I1'$	36	5.79×10^{-5}	1.73×10^{4}	0.89	1.54
	$A \rightarrow A'$	4	3.42×10^{-5}	2.92×10^{4}	0.39	1.48

[a]N_{traj} = number of trajectories following a particular mechanism.

Residue F4:

Residue F4 is located on the solvent-exposed protein exterior and has frequent interactions with residue R42. The free-energy surface is shown in Figure 2 together with representative structures. State A' and state I2' are considered "flipped" states, signaling that transition has occurred, thus providing τ_i $(i = 1\ to\ 40)$ values. The results are shown in **figure S13** and the

bootstrap analysis of all 40 τ_i values and the p-value obtained from the KS test are shown **in figure S14 in SI.** The effective t_{flip} considering all 40 simulations was 2.80×10^{-5} s.

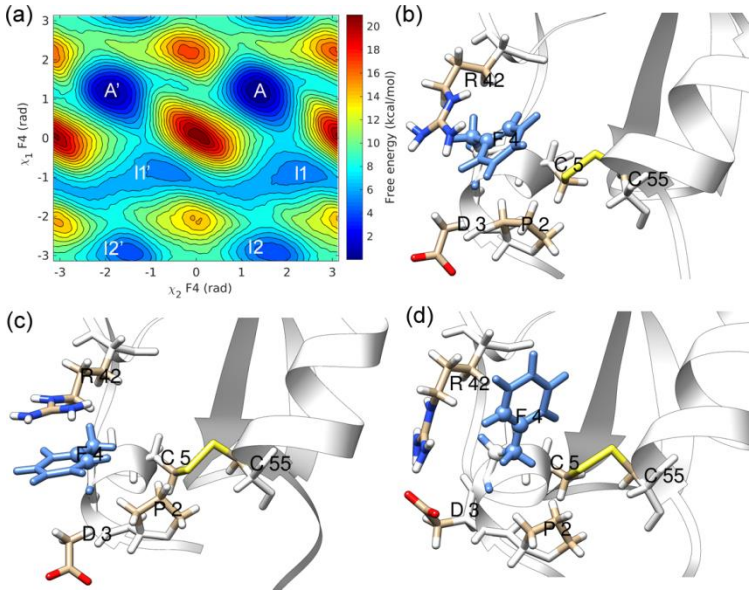

Figure 2. (a) Residue F4 (blue) ring-flipping free energy along χ_2 and χ_1 reaction coordinates and representative structures from (b) minimum A, (c) minimum I1, and (d) minimum I2.

State I1 is involved in the ring-flipping of residue F4. The cation-π interactions with positively charged residue R42 stabilizes the conformations in minimum I1. Residue F4 is located close to the disulfide bond [5-55] formed by C5 and C55. The disulfide bond [5-55] torsion was not affected during states A to I1 transition because the aromatic side-chain of F4 moved away from residue C5. State I2 has a trans orientation of the bonds N-CA (backbone) and CB-CG (side-chain), thus exposing R42 towards solvent. Salt bridge interactions were observed between R42 and D3 in state I2.

Three different mechanisms were observed during the InMetaD simulations, as described in Table 3. A to A' via intermediates is the prominent mechanism observed during F4 ring-flips. In this mechanism, ring-flips occur via coupled motions of the χ_2 and χ_1 torsions, starting from

state A, ring transit to state I1 multiple times, which acts as a steady-state before reaching state I1' and eventually proceed to A'. A direct ring flip from state A to A' was also observed, but these trajectories exhibited a few A to I1 reversible transitions before the direct transition. Finally, six trajectories flipped to state I2' while started from state A. Reversible transitions between states A and I1 were observed due to motions along χ_1. These trajectories represent an off-pathway mechanism where trajectories before proceeding to state I1' transition to state I2', thus achieving flipped orientation. Therefore, multiple flipping pathways are possible with almost the same t_{flip} in case of residue F4.

Residue Y10:

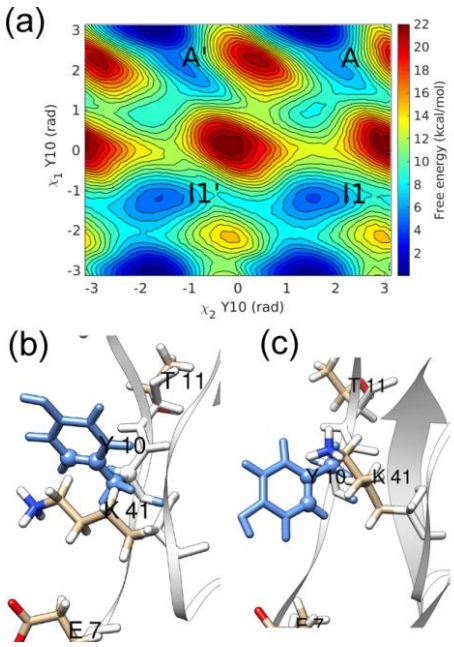

Figure 3. (a) $\chi_2 - \chi_1$ free energy surface, and representative structures in (b) minimum A and (c) minimum I1 of the free energy landscape of residue Y10 (blue).

We have observed two distinct mechanisms for flipping: a $\chi_2 - \chi_1$ coupled mechanism and a direct ring flip. The prominent mechanism of residue Y10 involves motions along the χ_1 torsion leading to stable state I1 (see figure 3(a)). In that state, residue Y10 is less restricted by

interactions with surrounding atoms (see fig. 3(c)) as the motions along χ_1 brings Y10 aromatic side-chain out of the core region surrounded by T11, K41, and P13. We have observed transient interactions with K41 but no hydrogen bonding interactions. The aromatic ring-flipping in Y10 illustrates an alternate mechanism to the "breathing cavity" mechanism proposed by earlier studies. This alternate mechanism involves moving the aromatic side-chain to the less crowded region and undergoing the flipping process. This mechanism is different from the "cavity model," where transient cavity formation allows ring-flipping.

Most InMetaD trajectories (36 out of 40 simulations) followed the $\chi_2 - \chi_1$ coupled mechanism involving state I1. A t_{flip} of $5.80 \times 10^{-5}\, s$ was observed by considering all 40 InMetaD simulations. The KS-test results and associated errors are reported in **figures S15 and S16 in SI.** Four trajectories have transitioned to flipped state *A'*. However, there were a few (one or two) A-I1 jumps that occurred before proceeding directly to state A'. Thus, state I1 is an important intermediate that could be an active or off-pathway state depending on the transition path.

Residue F33:

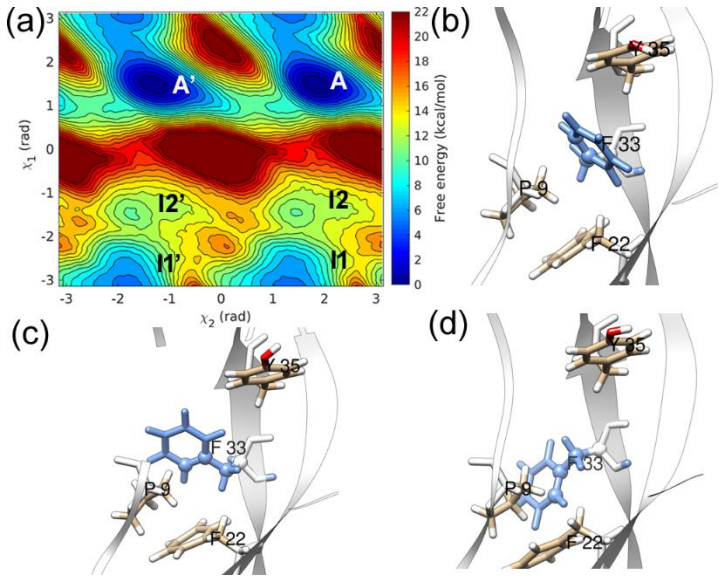

Figure 4. (a) $\chi_2 - \chi_1$ free energy surface, and representative structures in (b) minimum A, (c) minimum I1, and (d) minimum I2 of the free energy landscape of residue F33 (blue).

The residue F33 is surrounded by hydrophobic residues P9, F22, and Y35. The significant variation in values of χ_1 torsion during WTMetaD simulations leads to states I1 and I2, where the aromatic side-chain of F33 is out of the protein interior (see figure 4). The flipping of F33 only required small fluctuations relative to the backbone. Thus, even though states I1 and I2 were observed in the free energy landscape, the direct ring-flipping pathway did not involve these states. All trajectories visited an off-pathway state I1 during the InMetaD simulations. The F33 flipping affects χ_1 fluctuations of residue F22 (**see figure S17 in SI**). All InMetaD simulations showed flipping mainly by χ_2 rotation with positive values of χ_1 (**figure S11 in SI**). A t_{flip} of 3.50 $\times 10^{-5}$ s was obtained through the KS test and p-value of 0.03. To understand the small p-value, indicating significant deviation from the Poisson distribution, we analyzed the InMetaD trajectories and found deposition of bias in the barrier region along χ_1 ($\chi_1 \approx 2.4$ rad). The example of bias deposition in randomly chosen trajectories is shown in **figure S18** in the supporting information. Residue F33 demonstrated nonproductive off-pathway transitions between A and I1 states, whereas the main mechanism is direct flipping. To investigate whether these non-productive pathways affected the results, we performed another set of 12 InMetaD simulations, in which a repulsive wall bias restricted the sampling of χ_1 values greater than 2.4 rad (see method section). The t_{flip} value from 12 simulations with wall bias is close to previous $\chi_2 - \chi_1$ InMetaD simulations without wall bias (**see Table S2 and figures S19-S20 in SI**).

Slow flipping residues

Residue Y21 and F45:

As shown in Figure 5, residues Y21 and F45 both lack intermediates in the free energy surface and flip via a simple direct ring flip mechanism. Residue Y21 displayed convergence when only the χ_2 torsion was used as a CV and the resulting $t_{flip} = 5.20 \times 10^{-3}$ s would classify it as a slow-flipping residue. Residue Y21 is solvent-exposed, and thus simple motions along χ_2 torsion is sufficient as no steric hindrance with the surrounding protein matrix occurs. Instead, most of the ring flips occur in a narrow range of χ_1 values. The reweighted distribution of $\chi_2 - \chi_1$ from the converged metadynamics simulation indicates that no significant motions along χ_1 is needed, and Y21 can flip transiently. This residue lies on the rigid β-strand (I18-N24), which forms an anti-parallel β-sheet via strong interactions with another β-strand (L29-Y35). Interestingly residue F33 also lies on a β-strand but is a fast-flipping residue.

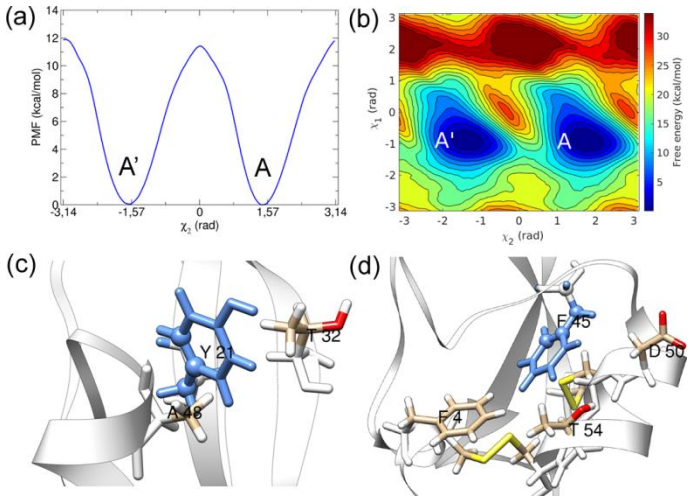

Figure 5. Free energy of (a) residue Y21 (blue) along χ_2, (b) residue F45 (blue) along $\chi_2 - \chi_1$, (c) representative structure from minimum A of residue Y21, and (d) from minimum A of residue F45.

A converged free energy surface was observed along $\chi_2 - \chi_1$ collective variables for residue F45, and thus, 40 InMetaD simulations were performed along the $\chi_2 - \chi_1$ variables. The distribution of τ_i (i=1 to 40) passes KS-test and fitted t_{flip} of 3.21 s was obtained, indicating F45 as a slow flipping residue. There is direct flipping in F45; however, χ_1 is needed for librational motions (see Fig. 5(d)), which facilitate flipping along χ_2 (*InMetaD simulations based on χ_2 did not pass the KS-test as discussed below*). The cumulative distribution function of τ_i and associated errors are shown in **figures S21 and S22 in SI.**

Residue F22:

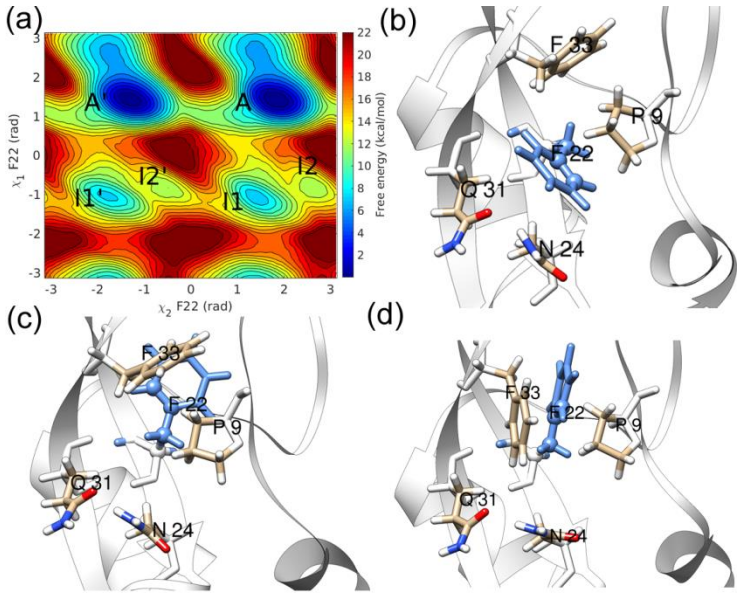

Figure 6. (a) Free energy of residue F22 (blue) along $\chi_2 - \chi_1$ and representative structure from (b) minimum A, (c) minimum I1, and (d) minimum I2.

Figure 6 shows the $\chi_2 - \chi_1$ free energy surface for F22 along with representative structures. All the InMetaD simulations followed a direct A → A' transition pathway as a high barrier exist along χ_1 to visit intermediate states. t_{flip} of 2.41×10^{-2} s was observed for a direct transition. Direct flip mechanism suggests residue F22 needs minimal fluctuations relative to the backbone

for ring-flipping and it might not be necessary to span the whole χ_1 torsion range, as observed in WTMetaD simulations. State I1 occurs due to changes χ_1 value and transient increase of the P9-F33 distance. In state I2, there is no stacking of F22 over F33, but these residues align approximately parallel to each other. During a long 1.6 μs WTMetaD simulation, we have observed a single ring flip event of residue F33 (**figure S23 in SI**). The KS-test results for residue F22 are reported in Figures **S24 and S25 in SI.**

Five InMetaD simulations in each case of (a) A → I1 pathway, (b) I1 → A pathway, and (c) I1 → I1' pathway were performed. In these simulations, the visits to other stable states were avoided using repulsive wall bias[41] using k and s_0 mentioned in **Table S3 in SI.** The results (**Table S4 in SI**) and details of these simulations are reported in **Appendix I in SI**. State-to-state transition rate matrix is reported in **Table S5 in SI**. The dominant eigenvalue 83 s^{-1} was estimated by solving this transition matrix.

Residue Y23:

Residue Y23 is one of the slowest flipping residues. The dynamics of ring Y23 was studied using the χ_2 torsion and a contact map of Cα atoms surrounding the ring (**figure S26 in SI**). The convergence in WTMetaD simulations and KS test validation assured the choice of CMAP as a CV complementary to χ_2. The transition is possible at CMAP values between 1 and 4, indicating that a small change in the equilibrium distances of Cα atoms is sufficient to provide the necessary volume for ring-flipping. Thus, a transient excited state could exist during ring-flipping, in which the surrounding atoms are not significantly displaced. We have performed 60 InMetaD simulations to obtain reliable statistics, and observed a t_{flip} of 0.98 s (see **Figures S27 and S28 in SI**).

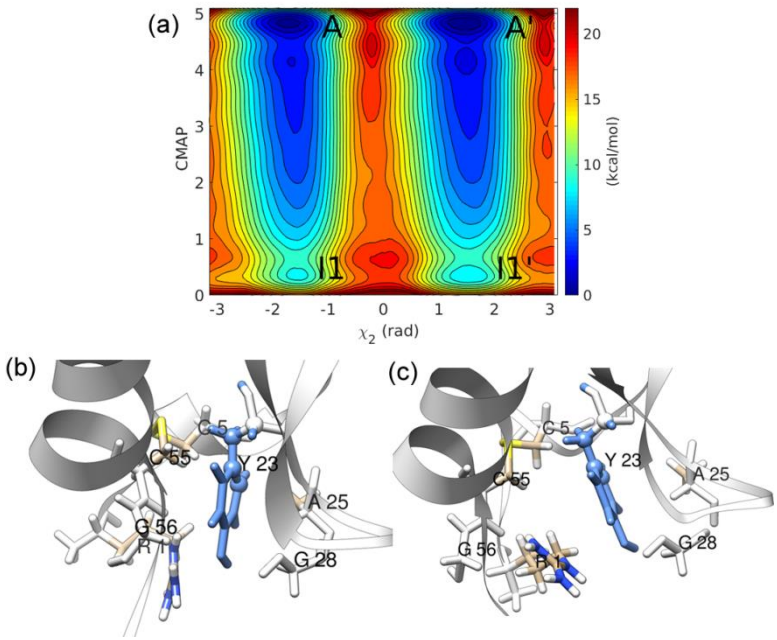

Figure 7. Free energy of (a) residue Y23 along $\chi_2 - CMAP$, and representative structure from (b) minimum A, and (c) minimum I1.

Residue Y23 is located near two disulfide bridges defined by residues 5-55 and 30-51. The aromatic side-chain of Y23 infrequently interacts with Cα, Sγ, N atom of residue C30 and backbone C, O atoms of residue C5. However, no significant changes in the values of χ_2, χ_1 and χ_3 torsions of the 5-55 and 30-51 disulfide bridges were observed (**figure S29 in SI**). Transient hydrogen bonds between residue Y23 and residues R1, G56, D3 were observed (**figure S30 in SI**). The fluctuations in the flexible residue R1 also transiently contributed to the cavity expansion due to interactions with residue G56. We have also performed $\chi_2 - \chi_1$ biased WTMetaD simulations; however, we observed a lack of convergence (**figures S31 and S32 in SI**). Visual observation of the WTMetaD simulation indicated a crowding effect of neighboring Cα atoms. Thus, a contact map was used as a complementary CV to obtain a converged free

energy landscape. Both $\chi_2 - \chi_1$ ($t_{flip} = 0.61$ s) and $\chi_2 - CMAP$ ($t_{flip} = 0.98$ s) InMetaD simulations provided similar t_{flip} values.

Karplus and Gelin[42] theoretically studied aromatic ring-flipping for Y10, Y21, Y23, and Y35 residues of BPTI by varying the χ_1 and χ_2 torsions. The study concluded that a few strong nonbonded interactions with surrounding atoms lead to a specific ring-flipping rate constant (k_{flip}) for each residue. In the DESRES simulation, the ring-flipping rate was not correlated with the density of heavy atoms within 4 Å of aromatic ring atoms at δ and ε positions[19]. This lack of correlation suggests no significant displacement of atoms surrounding the aromatic residue, contrary to the well-accepted cavity model.[12] We speculate that small displacements of a few surrounding atoms are sufficient to allow ring-flipping. The results for residue Y23 in this work support this hypothesis.

Residue Y35:

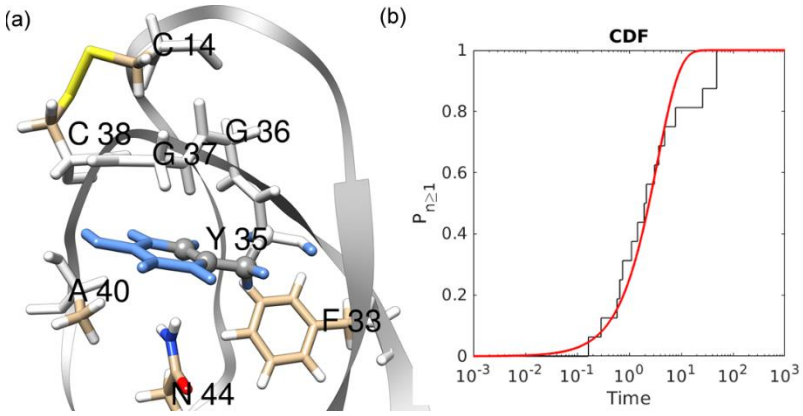

Figure 8. (a) Representative structure of residue Y35 in the native state, (b) Poisson fit to CDF of transition timescales obtained from $\chi_2 - \chi_1$ InMetaD simulations (p-value = 0.58 and μ ln 2/tm = 3.21).

Y35 is a slow flipping residue in BPTI and is one of the most studied aromatic side-chains by previous[10, 43-46] theoretical studies. The lack of converged free energy profiles for Y35 with χ_2 as

well as $\chi_2 - \chi_1$ biased metadynamics simulations indicates a missing orthogonal degree of freedom and probably a complex ring-flipping mechanism. Residue Y35 is located inside the protein core, close to the C14-C38 disulfide bond (figure 8), and near the initial part of the loop region formed by residues G36-A40. WTMetaD simulations along $\chi_2 - \chi_1$ (1.6 μs) and χ_2 (0.7 μs) for residue Y35 lacked convergence (**figures S7 and S8 in SI**). Thus, we speculate that more than two descriptors might be needed to understand the flipping of the Y35 aromatic side-chain.

The reweighted distribution of side-chain torsion χ_1 of C14 and C38 residues indicate that this simulation has sampled more than state M (**figure S33 in SI**). Thus, the loop region's conformations due to C14-C38 disulfide bond motions could affect the flipping rate.[19] We performed 16 InMetaD simulations, assuming $\chi_2 - \chi_1$ could provide rates in major state M1 and t_{flip} of 3.4 s was obtained, indicating Y35 as a slow flipping residue.

The disulfide bond isomerization could likely be associated with non-convergence of the $\chi_2 - \chi_1$ metadynamics simulations. Even in a 1-ms-long trajectory, multiple flipping rates of residue Y35 were reported based on C14-C38 disulfide bond isomerization[19]. Thus, we have also performed WTMetaD simulations with χ_2 and χ_1 of Y35, together with the χ_3 dihedral of the C14-C38 disulfide bond. This simulation demonstrated a free energy barrier of 6 kcal/mol for Y35 ring-flipping, as the Y35 aromatic side-chain is irreversibly expelled out of the protein core and was freely rotating in the solvent-exposed state (**figure S34 in SI**).

Recrossing events F22 and F33 ring-flipping

$\chi_2 - \chi_1$ biased InMetaD simulations of residues F22 and F33 demonstrated recrossing events. In figure 9, we have presented one such trajectory of residue F33 to understand the structural details of recrossing. In this trajectory, the first attempt of ring-flipping occurred around 22538

ps (figure 9(b)), when the χ_2 value reached -2.06 rad while maintaining positive χ_1 values (state R).

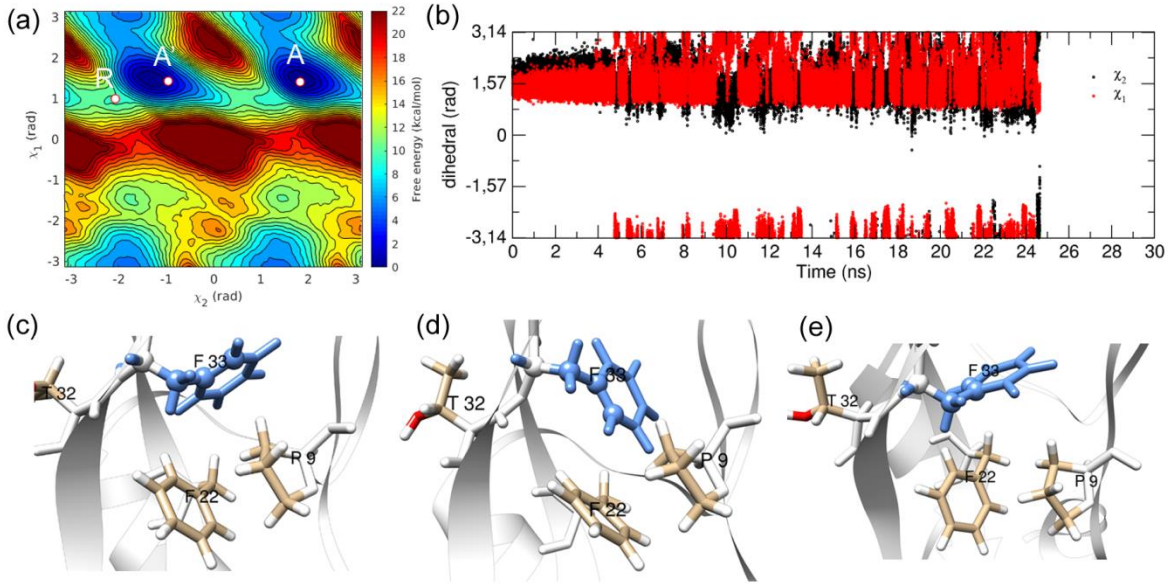

Figure 9. Representative InMetaD trajectory showing recrossing event in F33 ring-flipping. (a) the starting state ***A*** , flipped state ***A'*** , and point of recrossing ***R*** on the free energy surface of $\chi_2 - \chi_1$, (b) time evolution of χ_2 and χ_1 torsion angles, (c) orientation of F33 in the native state(state *A*, χ_2 = 1.83 rad, χ_1= 1.41 rad), (d) structure at 22538 ps (state *R*, χ_2 = -2.06 rad, χ_1=0.99 rad) , (e) flipped state at 24643 ps (state *A'* , χ_2=-0.95 rad, χ_1 = 1.42 rad).

$\chi_2 - \chi_1$biased InMetaD simulations of residues F22 and F33 demonstrated recrossing events. In figure 9, we have presented one such trajectory of residue F33 to understand the structural details of recrossing. In this trajectory, the first attempt of ring-flipping occurred around 22538 ps (figure 9(b)), when the χ_2 value reached -2.06 rad while maintaining positive χ_1 values (state R). The ring rotates back to positive χ_2 values after this state and keeps sampling in the initial region with a few *A*-*I*1 transitions. Transition state theory[47-48] (TST) assumes that the trajectories cross the barrier region (which divides the reactant and product states) and continue to the

product state. TST-based transition rate (k_{TST}) can be calculated from the free energy of activation ($\Delta G^{\ddagger}$) using the Eyring equation [10].

$$k_{TST} = \frac{k_B T}{h} e^{\frac{-\Delta G^{\ddagger}}{RT}} \qquad [10]$$

where k_B is Boltzmann's constant, T is the temperature, h is Planck's constant, and R is the gas constant. The TST-based rate due to recrossing events is corrected using the transmission coefficient (κ):

$$k_{true} = \kappa k_{TST} \quad [11]$$

The origin[48-49] of recrossing events could be associated with the efficiency of collective variables to describe the transition state or with strong coupling between system coordinates undergoing transition and the surrounding environment. However, it is complicated to define the precise TS. Thus, according to variational TST[48-49], an optimized reaction coordinate that minimizes recrossing events should be defined to understand dynamics. For residue F22, a barrier of 12 kcal/mol exists along the direct flipping pathway, thus estimating the ring-flipping rate, $k_{TST} = 1.13 \times 10^4\ s^{-1}$, according to equation [10]. If collective variables χ_2 and χ_1 are speculated to capture the dynamics of F22 ring-flipping correctly, then the true rate of ring-flip (k_{true}) is the same as the one obtained from InMetaD simulations ($k_{InMetaD}$) i.e. $k_{true} = k_{InMetaD}$. The substitution of k_{TST} and $k_{InMetaD}$ values in equation [11] then suggests that $\kappa = 3.67 \times 10^{-3}$.

Based on the variational TST assumption, this unusually low transmission coefficient κ value could be attributed to the choice of CVs, χ_2 and χ_1, used for InMetaD simulations. To verify this assumption, we performed 12 InMetaD simulations in each case of residue F22 and F33 using reaction coordinates optimized using a variational approach (VAC-MetaD).[37] This approach allows a linear combination of multiple descriptors of the process and enables a better

description of transition states and stable states. We have considered the distance between residues P9 and F33, χ_1 and χ_2 torsions of residues F22 and F33 to build VAC-optimized CVs (VAC-CVs). The computational details and results of these simulations are reported in the SI (**Appendix II in SI**).

With VAC-CVs, t_{flip} values 0.09 s (p-value = 0.49) and 8.64×10^{-5} s (p-value=0.70) were obtained for residues F22 and F33, respectively (**figure S47 in SI**). Thus, even with optimized CVs, residue F22 gave a low κ value. Furthermore, we have also observed recrossing events in a few F22 and F33 VAC-CV based simulations. Thus, further analysis is needed to understand the origin of such low transmission coefficient and the corresponding frictional effects. A recrossing event was also observed for c36 based InMetaD simulations of F22.

Limitations of 1D χ_2 InMetaD simulations:

Table 4. χ_2 biased InMetaD derived ring flip rate ($\boldsymbol{k_{\chi_2}}$) at 300 K, number of simulations (N), KS-test derived the ratio of average (μ) to the median of Poisson distribution and p-value, InMetaD simulation parameters hill height (w, kJ.mol^{-1}), bias factor (γ), frequency of hill addition (ν , ps).

Residue	$\boldsymbol{k_{\chi_2}}$ $(\boldsymbol{s^{-1}})$	N	$(\boldsymbol{\mu \ln 2})/\boldsymbol{t_m}$	$\boldsymbol{p}$-value	γ	w	ν
F4	3.44×10^4	12	2.98	0.86	15	1.2	12
Y10	5.88×10^2	40	1.79	0.21	10	0.6	18
Y21	1.92×10^2	40	1.32	0.68	10	0.6	18
F22	3.65	20	2.94	0.45	8	1.2	12
Y23	4.0×10^{-2}	12	3.71	0.02	12	1.2	12
F33	3.4×10^4	15	3.46	0.90	12	0.6	10
F45	1.2×10^{-1}	40	5.39	0.00	10	0.6	18

We performed InMetaD simulations biasing χ_2 as a standalone CV to understand its limitations and accuracy to estimate t_{flip} values. The details of metadynamics parameters and the outcome of χ_2 biased InMetaD runs are reported in **Table 4**. KS test results for all residues are reported in **figures S39 and S40 in SI.** χ_2 biased InMetaD simulations were not performed for residue Y35, as WTMetaD simulations biasing χ_2 of Y35 lacked frequent ring-flip events (**figure S8 in SI**).

χ_2 biased WTMetaD simulations for all residues, except Y21, lacked convergence. An example is shown in **figure S41 in SI** for residue Y10. The slow diffusion of χ_2 and χ_1 of residue Y10 in χ_2 biased WTMetaD simulation suggests that biasing of both CVs is necessary. InMetaD simulations along χ_2 for residue Y10 yielded t_{flip} values two orders of magnitude slower than $\chi_2 - \chi_1$ InMetaD. We observed that most of these trajectories had a direct transition from state *A* to *A'* with no significant fluctuations along the χ_1 torsion. This result shows that biased CVs direct the reactive flux along pathways specific to them and could provide different timescales. χ_2 biased InMetaD simulations demonstrate that t_{flip} could be overestimated if diffusion along other relevant degrees of freedom is neglected in InMetaD. It is noteworthy that both χ_2 and χ_2-χ_1 biased InMetaD simulations of residue Y10 passed the KS-test and has low $(\mu \ln 2)/t_m$ ratio. In general, missing descriptors of the process could affect the metadynamics derived t_{flip} values even if the two-sample KS test is passed. Theoretically, multiple CVs are needed to capture all metastable states on the free energy landscape. Thus, recent machine learning-based methods to define a combination of multiple collective variables could be specifically useful to obtain reliable rates with InMetaD.

For residue F22, the InMetaD simulations with the χ_2 torsion passed the KS test but prediected t_{flip} an order of magnitude slower than the $\chi_2 - \chi_1$ InMetaD simulations. Interestingly, both types of simulations (χ_2 and $\chi_2 - \chi_1$ InMetaD) gave much higher t_{flip} values than observed in the DESRES trajectory. For residue F45, distribution of τ_i values from the χ_2 InMetaD simulations (**figure S40 in SI**) indicated deviation (p-value of 0.00) from ideal Poisson distribution (although the t_{flip} value obtained from these simulations is comparable with the value obtained from $\chi_2 - \chi_1$ InMetaD simulations). This exemplifies that apart from collective variables that discriminate stable states, the CVs which promote the diffusion of such principal CVs are needed for reliable estimation of dynamics from metadynamics.

CHARMM simulations

We have performed metadynamics simulations using two CHARMM36 force field variants, c36, and c36m, as described in the section, for residue F22 with χ_2 and χ_1 collective variables. The free energy barriers along χ_1 are 3 kcal/mol lower compared to the AMBER ff14SB force field. The convergence of these simulations is reported in SI (**figures S42 and S43**).

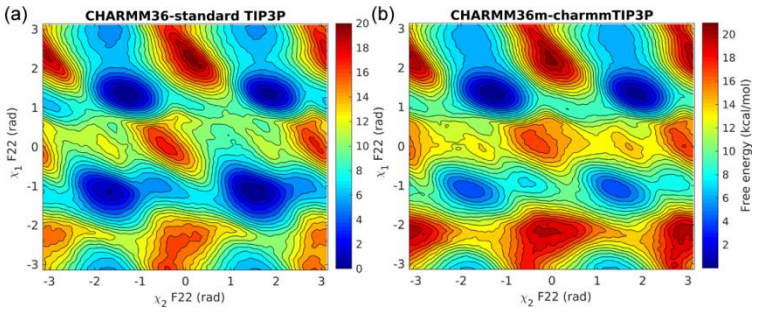

Figure 10. (a) The free energy landscape of residue F22 along $\chi_2 - \chi_1$ collective variables with (a) CHARMM36 and TIP3P water model and (b) CHARMM36m and modified TIP3P water model.

The ring flip timescales were estimated for residues F22 (16 simulations) and F45 (12 simulations) modeled with the c36 force field. For residues F22 and F45, t_{flip} values of 5.45×10^{-4} s ($k_{flip} = 1.83 \times 10^{3}\ s^{-1}$, p-value=0.69) and 1.78×10^{-1} s ($k_{flip} = 5.61\ s^{-1}$, p-value = 0.97) were observed, respectively, predicting slow flipping residues(**figure S44 in SI**), but faster by 1-2 orders of magnitude than AMBER ff14SB. The barrier of 9.0 kcal/mol for F22 suggests $k_{TST} = 1.74 \times 10^{6}\ s^{-1}$, thus giving (again) a low κ value of 1.04×10^{-3} for the c36 based F22 InMetaD simulations.

CONCLUSIONS

In the present work, we describe a metadynamics based approach to calculate the ring flipping rate and mechanism for eight individual aromatic rings in BPTI. We utilized the InMetaD method to obtain first passage times (τ_i) to estimate t_{flip}. This approach successfully distinguished between experimentally categorized "slow" and "fast" residues with an appropriate choice of CVs. Our InMetaD simulations categorized residues F4, F33, Y10 as fast flipping and residues Y21, F22, Y23, F45, and Y35 as slow flipping residues. Resides Y35, Y23, and F45 exhibited timescales up to seconds, significantly slower than millisecond brute-force simulation. The rank order observed for ring flips from slow to fast is as follows: F45 < Y23, Y35 < Y21, F22 < Y10 < F4, F33. Indeed, NMR measurements and 1-ms-long simulation[3, 19] observed residues F33 and F4 as fast flipping residues. We also investigated the correlation between solvent accessible surface area (SASA) of aromatic side-chains and experimental ring-flipping rates k_{exp}, however, a lack of correlation was observed similar to the previous study[50] (**figure S37** in SI). The free energy surface of solvent-exposed residues (F4, Y10) and buried residues (F22, F33, Y35) indicated multiple ring-flipping pathways. The circular correlation coefficient[51] between χ_1, χ_2 dihedrals of eight aromatic residues obtained from 1-ms-long trajectory indicate

no correlated motions between these residues (**figure S38 in SI**). The side-chain aromatic ring of residues Y23 and F45 flips around seconds; these time scales are still beyond the scope of present MD simulations. This study illustrates that InMetaD can be applied to understand motions occurring at second time scales, as also demonstrated by drug-unbinding studies[52-54]. The InMetaD simulations of residues F33 and F22 indicate friction effects during barrier crossing events. Further investigations is needed to understand the origin of these observations. This study illustrates the complexity of the ring flipping process in globular proteins.

ASSOCIATED CONTENT

Supporting Information. The Supporting Information is available free of charge at ...

A convergence of WTMetaD simulations, results of χ_2 InMetaD simulations, distribution of side-chain torsions of a C14-C38 disulfide bond, SASA results, circular cross-correlation of χ_2 and χ_1 dihedral values obtained from 1-ms-long D. E. Shaw Research (DESRES) trajectory, details of state-to-state transitions of residue F22, and details of VAC-metadynamics simulations.

AUTHOR INFORMATION

Corresponding Author

*E-mail: mandar.kulkarni.chem@gmail.com; par.soderhjelm@bpc.lu.se

ORCID

Mandar Kulkarni: 0000-0002-9005-9553

Pär Söderhjelm: 0000-0001-6938-7803

Author Contributions

The manuscript was written through the contributions of all authors. All authors have given approval to the final version of the manuscript.

Funding Resources

PS acknowledges funding from the Swedish Research council (project 2017-05318). The computations were performed on resources provided by SNIC through LUNARC at Lund University and HPC2N at Umeå University under Projects SNIC 2019/3-317 and SNIC 2020/5-367.

Notes

The authors declare no competing financial interest.

ACKNOWLEDGMENT

M.K. thanks Dr. Yong Wang, Department of Biology, the University of Copenhagen, for providing bootstrap analysis Matlab script of transition timescales.

References:

1. Shortle, D.; Simons, K. T.; Baker, D., Clustering of low-energy conformations near the native structures of small proteins. *Proc. Natl. Acad. Sci. U.S.A.* **1998,** *95* (19), 11158-11162.
2. Kasinath, V.; Fu, Y.; Sharp, K. A.; Wand, A. J., A Sharp Thermal Transition of Fast Aromatic-Ring Dynamics in Ubiquitin. *Angew. Chem.* **2015,** *54* (1), 102-107.
3. Weininger, U.; Modig, K.; Akke, M., Ring Flips Revisited: 13C Relaxation Dispersion Measurements of Aromatic Side Chain Dynamics and Activation Barriers in Basic Pancreatic Trypsin Inhibitor. *Biochemistry* **2014,** *53* (28), 4519-4525.
4. Wüthrich, K.; Wagner, G., NMR investigations of the dynamics of the aromatic amino acid residues in the basic pancreatic trypsin inhibitor. *FEBS Lett.* **1975,** *50* (2), 265-268.
5. Wagner, G.; DeMarco, A.; Wüthrich, K., Dynamics of the aromatic amino acid residues in the globular conformation of the basic pancreatic trypsin inhibitor (BPTI). *Biophys. Struct. Mech.* **1976,** *2* (2), 139-158.

6. Li, H.; Yamada, H.; Akasaka, K., Effect of Pressure on the Tertiary Structure and Dynamics of Folded Basic Pancreatic Trypsin Inhibitor. *Biophys. J.* **1999,** *77* (5), 2801-2812.
7. Krishna Rao, D.; Bhuyan, A. K., Complexity of aromatic ring-flip motions in proteins: Y97 ring dynamics in cytochrome c observed by cross-relaxation suppressed exchange NMR spectroscopy. *J. Biomol. NMR* **2007,** *39* (3), 187-196.
8. Wagner, G.; Brühwiler, D.; Wüthrich, K., Reinvestigation of the aromatic side-chains in the basic pancreatic trypsin inhibitor by heteronuclear two-dimensional nuclear magnetic resonance. *J. Mol. Biol* **1987,** *196* (1), 227-231.
9. Wagner, G., Activation volumes for the rotational motion of interior aromatic rings in globular proteins determined by high resolution 1H NMR at variable pressure. *FEBS Lett.* **1980,** *112* (2), 280-284.
10. Karplus, M.; Gelin, B. R.; McCammon, J. A., Internal dynamics of proteins. Short time and long time motions of aromatic sidechains in PTI. *Biophys. J.* **1980,** *32* (1), 603-618.
11. Weininger, U.; Respondek, M.; Löw, C.; Akke, M., Slow Aromatic Ring Flips Detected Despite Near-Degenerate NMR Frequencies of the Exchanging Nuclei. *J. Phys. Chem. B* **2013,** *117* (31), 9241-9247.
12. Hattori, M.; Li, H.; Yamada, H.; Akasaka, K.; Hengstenberg, W.; Gronwald, W.; Kalbitzer, H. R., Infrequent cavity-forming fluctuations in HPr from Staphylococcus carnosus revealed by pressure- and temperature-dependent tyrosine ring flips. *Protein Science* **2004,** *13* (12), 3104-3114.
13. Wagner, G., Characterization of the distribution of internal motions in the basic pancreatic trypsin inhibitor using a large number of internal NMR probes. *Quarterly Reviews of Biophysics* **2009,** *16* (1), 1-57.
14. Karplus, M.; McCammon, J. A., Pressure dependence of aromatic ring rotations in proteins: a collisional interpretation. *FEBS Letters* **1981,** *131* (1), 34-36.
15. Zhang, J.-X.; Goldenberg, D. P., Mutational analysis of the BPTI folding pathway: I. Effects of aromatic → leucine substitutions on the distribution of folding intermediates. *Protein Sci.* **1997,** *6* (7), 1549-1562.
16. Yu, M. H.; Weissman, J. S.; Kim, P. S., Contribution of individual side-chains to the stability of BPTI examined by alanine-scanning mutagenesis. *J. Mol. Biol* **1995,** *249* (2), 388-97.
17. Islam, M. M.; Sohya, S.; Noguchi, K.; Yohda, M.; Kuroda, Y., Crystal structure of an extensively simplified variant of bovine pancreatic trypsin inhibitor in which over one-third of the residues are alanines. *Proc. Natl. Acad. Sci. U.S.A.* **2008,** *105* (40), 15334-15339.
18. Gall, C. M.; DiVerdi, J. A.; Opella, S. J., Phenylalanine ring dynamics by solid-state deuterium NMR. *J. Am. Chem. Soc.* **1981,** *103* (17), 5039-5043.
19. Shaw, D. E.; Maragakis, P.; Lindorff-Larsen, K.; Piana, S.; Dror, R. O.; Eastwood, M. P.; Bank, J. A.; Jumper, J. M.; Salmon, J. K.; Shan, Y.; Wriggers, W., Atomic-Level Characterization of the Structural Dynamics of Proteins. *Science* **2010,** *330* (6002), 341-346.
20. Barducci, A.; Bussi, G.; Parrinello, M., Well-Tempered Metadynamics: A Smoothly Converging and Tunable Free-Energy Method. *Phys. Rev. Lett.* **2008,** *100* (2), 020603.
21. Laio, A.; Parrinello, M., Escaping free-energy minima. *Proc. Natl. Acad. Sci. U.S.A.* **2002,** *99* (20), 12562-12566.
22. Tiwary, P.; Parrinello, M., From Metadynamics to Dynamics. *Phys. Rev. Lett.* **2013,** *111* (23), 230602.
23. Sousa da Silva, A. W.; Vranken, W. F., ACPYPE - AnteChamber PYthon Parser interfacE. *BMC Res. Notes* **2012,** *5* (1), 367.

24. Maier, J. A.; Martinez, C.; Kasavajhala, K.; Wickstrom, L.; Hauser, K. E.; Simmerling, C., ff14SB: Improving the Accuracy of Protein Side Chain and Backbone Parameters from ff99SB. *J. Chem. Theory Comput.* **2015,** *11* (8), 3696-3713.
25. Horn, H. W.; Swope, W. C.; Pitera, J. W.; Madura, J. D.; Dick, T. J.; Hura, G. L.; Head-Gordon, T., Development of an improved four-site water model for biomolecular simulations: TIP4P-Ew. *J. Chem. Phys.* **2004,** *120* (20), 9665-9678.
26. Joung, I. S.; Cheatham, T. E., Determination of Alkali and Halide Monovalent Ion Parameters for Use in Explicitly Solvated Biomolecular Simulations. *J. Phys. Chem. B* **2008,** *112* (30), 9020-9041.
27. Berendsen, H. J. C.; Postma, J. P. M.; van Gunsteren, W. F.; DiNola, A.; Haak, J. R., Molecular dynamics with coupling to an external bath. *J. Chem. Phys.* **1984,** *81* (8), 3684-3690.
28. Parrinello, M.; Rahman, A., Polymorphic transitions in single crystals: A new molecular dynamics method. *J. Appl. Phys.* **1981,** *52* (12), 7182-7190.
29. Bussi, G.; Donadio, D.; Parrinello, M., Canonical sampling through velocity rescaling. *J. Chem. Phys.* **2007,** *126* (1), 014101.
30. Kutzner, C.; Páll, S.; Fechner, M.; Esztermann, A.; de Groot, B. L.; Grubmüller, H., More bang for your buck: Improved use of GPU nodes for GROMACS 2018. *J. Comput. Chem.* **2019,** *40* (27), 2418-2431.
31. Abraham, M. J.; Murtola, T.; Schulz, R.; Páll, S.; Smith, J. C.; Hess, B.; Lindahl, E., GROMACS: High performance molecular simulations through multi-level parallelism from laptops to supercomputers. *SoftwareX* **2015,** *1-2*, 19-25.
32. Bonomi, M.; Branduardi, D.; Bussi, G.; Camilloni, C.; Provasi, D.; Raiteri, P.; Donadio, D.; Marinelli, F.; Pietrucci, F.; Broglia, R. A.; Parrinello, M., PLUMED: A portable plugin for free-energy calculations with molecular dynamics. *Comput. Phys. Commun* **2009,** *180* (10), 1961-1972.
33. Bonomi, M.; Bussi, G.; Camilloni, C.; Tribello, G. A.; Banáš, P.; Barducci, A.; Bernetti, M.; Bolhuis, P. G.; Bottaro, S.; Branduardi, D.; Capelli, R.; Carloni, P.; Ceriotti, M.; Cesari, A.; Chen, H.; Chen, W.; Colizzi, F.; De, S.; De La Pierre, M.; Donadio, D.; Drobot, V.; Ensing, B.; Ferguson, A. L.; Filizola, M.; Fraser, J. S.; Fu, H.; Gasparotto, P.; Gervasio, F. L.; Giberti, F.; Gil-Ley, A.; Giorgino, T.; Heller, G. T.; Hocky, G. M.; Iannuzzi, M.; Invernizzi, M.; Jelfs, K. E.; Jussupow, A.; Kirilin, E.; Laio, A.; Limongelli, V.; Lindorff-Larsen, K.; Löhr, T.; Marinelli, F.; Martin-Samos, L.; Masetti, M.; Meyer, R.; Michaelides, A.; Molteni, C.; Morishita, T.; Nava, M.; Paissoni, C.; Papaleo, E.; Parrinello, M.; Pfaendtner, J.; Piaggi, P.; Piccini, G.; Pietropaolo, A.; Pietrucci, F.; Pipolo, S.; Provasi, D.; Quigley, D.; Raiteri, P.; Raniolo, S.; Rydzewski, J.; Salvalaglio, M.; Sosso, G. C.; Spiwok, V.; Šponer, J.; Swenson, D. W. H.; Tiwary, P.; Valsson, O.; Vendruscolo, M.; Voth, G. A.; White, A.; The, P. c., Promoting transparency and reproducibility in enhanced molecular simulations. *Nat. Methods* **2019,** *16* (8), 670-673.
34. Tribello, G. A.; Bonomi, M.; Branduardi, D.; Camilloni, C.; Bussi, G., PLUMED 2: New feathers for an old bird. *Comput. Phys. Commun* **2014,** *185* (2), 604-613.
35. Tiwary, P.; Dama, J. F.; Parrinello, M., A perturbative solution to metadynamics ordinary differential equation. *The Journal of Chemical Physics* **2015,** *143* (23), 234112.
36. Tiwary, P.; Parrinello, M., A Time-Independent Free Energy Estimator for Metadynamics. *J. Phys. Chem. B* **2015,** *119* (3), 736-742.
37. McCarty, J.; Parrinello, M., A variational conformational dynamics approach to the selection of collective variables in metadynamics. *J. Chem. Phys.* **2017,** *147* (20), 204109.

38. Grey, M. J.; Wang, C.; Palmer, A. G., Disulfide Bond Isomerization in Basic Pancreatic Trypsin Inhibitor: Multisite Chemical Exchange Quantified by CPMG Relaxation Dispersion and Chemical Shift Modeling. *J. Am. Chem. Soc.* **2003,** *125* (47), 14324-14335.
39. Otting, G.; Liepinsh, E.; Wuethrich, K., Disulfide bond isomerization in BPTI and BPTI(G36S): An NMR study of correlated mobility in proteins. *Biochemistry* **1993,** *32* (14), 3571-3582.
40. Salvalaglio, M.; Tiwary, P.; Parrinello, M., Assessing the Reliability of the Dynamics Reconstructed from Metadynamics. *J. Chem. Theory Comput.* **2014,** *10* (4), 1420-1425.
41. Fu, C. D.; Oliveira, L. F. L.; Pfaendtner, J., Determining energy barriers and selectivities of a multi-pathway system with infrequent metadynamics. *J. Chem. Phys.* **2017,** *146* (1), 014108.
42. Gelin, B. R.; Karplus, M., Sidechain torsional potentials and motion of amino acids in porteins: bovine pancreatic trypsin inhibitor. *Proc. Natl. Acad. Sci. U.S.A.* **1975,** *72* (6), 2002-2006.
43. Northrup, S. H.; Pear, M. R.; Lee, C. Y.; McCammon, J. A.; Karplus, M., Dynamical theory of activated processes in globular proteins. *Proc. Natl. Acad. Sci. U.S.A.* **1982,** *79* (13), 4035-4039.
44. McCammon, J. A.; Lee, C. Y.; Northrup, S. H., Side-chain rotational isomerization in proteins: a mechanism involving gating and transient packing defects. *J. Am. Chem. Soc.* **1983,** *105* (8), 2232-2237.
45. Ghosh, I.; McCammon, J. A., Sidechain rotational isomerization in proteins. Dynamic simulation with solvent surroundings. *Biophys. J.* **1987,** *51* (4), 637-641.
46. Karplus, M., Aspects of Protein Reaction Dynamics: Deviations from Simple Behavior. *J. Phys. Chem. B* **2000,** *104* (1), 11-27.
47. Eyring, H., The Activated Complex and the Absolute Rate of Chemical Reactions. *Chem. Rev.* **1935,** *17* (1), 65-77.
48. Truhlar, D. G., Transition state theory for enzyme kinetics. *Arch. Biochem. Biophys.* **2015,** *582*, 10-17.
49. Tuñón, I.; Laage, D.; Hynes, J. T., Are there dynamical effects in enzyme catalysis? Some thoughts concerning the enzymatic chemical step. *Arch. Biochem. Biophys.* **2015,** *582*, 42-55.
50. Skalicky, J. J.; Mills, J. L.; Sharma, S.; Szyperski, T., Aromatic Ring-Flipping in Supercooled Water: Implications for NMR-Based Structural Biology of Proteins. *J. Am. Chem. Soc.* **2001,** *123* (3), 388-397.
51. Fenwick, R. B.; Orellana, L.; Esteban-Martín, S.; Orozco, M.; Salvatella, X., Correlated motions are a fundamental property of β-sheets. *Nat. Commun.* **2014,** *5* (1), 4070.
52. Tiwary, P.; Limongelli, V.; Salvalaglio, M.; Parrinello, M., Kinetics of protein–ligand unbinding: Predicting pathways, rates, and rate-limiting steps. *Proc. Natl. Acad. Sci. U.S.A.* **2015,** *112* (5), E386-E391.
53. Tiwary, P.; Mondal, J.; Berne, B. J., How and when does an anticancer drug leave its binding site? *Sci. Adv.* **2017,** *3* (5), e1700014.
54. Casasnovas, R.; Limongelli, V.; Tiwary, P.; Carloni, P.; Parrinello, M., Unbinding Kinetics of a p38 MAP Kinase Type II Inhibitor from Metadynamics Simulations. *J. Am. Chem. Soc.* **2017,** *139* (13), 4780-4788.

For Table of Contents Only